Intra-Cation versus Inter-Cation π-Contacts in [Cu(P^P)(N^N)][PF$_6$] Complexes

Francesca Mazzeo, Fabian Brunner, Alessandro Prescimone, Edwin C. Constable and Catherine E. Housecroft *

Department of Chemistry, University of Basel, BPR 1096, Mattenstrasse 24a, CH-4058 Basel, Switzerland; francesca.mazzeo@unibas.ch (F.M.); fabian.brunner@unibas.ch (F.B.); alessandro.prescimone@unibas.ch (A.P.); edwin.constable@unibas.ch (E.C.C.)

* Correspondence: catherine.housecroft@unibas.ch; Tel.: +41-61-207-1008

Abstract: A series of [Cu(POP)(N^N)[PF$_6$] and [Cu(xantphos)(N^N)][PF$_6$] compounds has been prepared and characterized in which POP = bis[2-(diphenylphosphanyl)phenyl]ether (IUPAC PIN oxydi(2,1-phenylene)bis(diphenylphosphane), xantphos = 4,5-bis(diphenylphosphanyl)-9,9-dimethyl-9*H*-xanthene (IUPAC PIN (9,9-dimethyl-9*H*-xanthene- 4,5-diyl)bis(diphenylphosphane)) and the N^N ligands are 4-(4-bromophenyl)-6,6′-dimethyl-2,2′- bipyridine (**1**), 5,5′-bis(3-methoxyphenyl)-6-methyl-2,2′-bipyridine (**2**), and 6-benzyl-2,2′-bipyridine (**3**). The single crystal structures of [Cu(xantphos)(**1**)][PF$_6$]·CH$_2$Cl$_2$, [Cu(xantphos)(**2**)][PF$_6$]·CH$_2$Cl$_2$ and [Cu(POP)(**3**)][PF$_6$]·0.5H$_2$O were determined by X-ray diffraction. Each complex contains a copper(I) ion in a distorted tetrahedral environment with chelating N^N and P^P ligands. In the [Cu(xantphos)(**1**)]$^+$ and [Cu(xantphos)(**2**)]$^+$ cations, there are face-to-face π-stackings of bpy and PPh$_2$ phenyl rings (i.e., between the ligands); in addition in [Cu(xantphos)(**2**)][PF$_6$]·CH$_2$Cl$_2$, inter-cation π-embraces lead to the formation of infinite chains as a primary packing motif. In [Cu(POP)(**3**)][PF$_6$]·0.5H$_2$O, centrosymmetric pairs of [Cu(POP)(**3**)]$^+$ cations engage in C–H . . . π (phenyl to bpy) and offset face-to-face (bpy . . . bpy) contacts. The electrochemical and photophysical properties of the compounds containing ligands **1** and **2** are reported. They are green or yellow emitters in the solid-state (λ_{em} in the range 535–577 nm) with values for the photoluminescence quantum yield (PLQY) in the range 19%–41%.

Keywords: copper(I); bis(phosphane); 2,2′-bipyridine; heteroleptic complex; X-ray crystallography; emission

1. Introduction

Over the last decade, interest has grown in the use of [Cu(P^P)(N^N)]$^+$ complexes (N^N = diimine, P^P = bisphosphane) in the emissive layers of light-emitting electrochemical cells [1–5]. This family of luminescent materials has been developed from the work of McMillin and co-workers who were the first to observe that copper(I) complexes containing both bisphosphane or PPh$_3$ ligands and 2,2′-bipyridine (bpy) or 1,10-phenanthroline (phen) exhibited low-lying metal-to-ligand charge transfer (MLCT) excited states [6,7]. [Cu(P^P)(N^N)]$^+$ complexes containing the wide bite-angle bisphosphanes 4,5-bis(diphenylphosphanyl)-9,9-dimethyl-9*H*-xanthene (xantphos, IUPAC PIN (9,9-dimethyl-9*H*-xanthene-4,5-diyl)bis(diphenylphosphane)) and bis(2-(diphenylphosphanyl)phenyl)ether (POP, IUPAC PIN oxydi(2,1-phenylene)]bis(diphenylphosphane)) (Scheme 1) have been widely investigated and show particular promise as materials exhibiting high photoluminescence quantum yields (PLQYs).

In our own investigations, we have focused mainly on [Cu(POP)(NˆN)]$^+$ and [Cu(xantphos)(NˆN)]$^+$ complexes in which NˆN is a 6-Xbpy or 6,6'-X$_2$bpy in which X is an alkyl [8,9], alkyloxy [10], alkylthio [10], aryl [9,11], halo [12] or trifluoroalkyl [13] substituent. Some of the highest values of PLQY for solid-state compounds have been observed for [Cu(xantphos)(6-Mebpy)][PF$_6$] (34%), [Cu(xantphos)(6-Etbpy)][PF$_6$] (37%), [Cu(xantphos)(6,6'-Me$_2$bpy)][PF$_6$] (37%) [9] and [Cu(xantphos)(6-PhSbpy)][PF$_6$] (38%) (6-Mebpy = 6-methyl-2,2'-bipyridine, 6-Etbpy = 6-ethyl-2,2'-bipyridine, 6,6'-Me$_2$bpy = 6,6'-methyl-2,2'-bipyridine, 6-PhSbpy = 6-phenylthio-2,2'-bipyridine) [10]. A recurring feature of the solid-state structures of [Cu(xantphos)(6-Xbpy)]$^+$ complexes is the accommodation of the X group within the bowl-shaped cavity of the xanthene unit.

Armaroli, Nierengarten, Delavaux-Nicot, and coworkers have demonstrated that in [Cu(PˆP)(phen)]$^+$ and [Cu(PˆP)(4,7-Ph$_2$phen)]$^+$ (4,7-Ph$_2$phen = 4,7-diphenyl-1,10-phenanthroline) complexes, a factor which contributes to enhanced PLQY is the presence of intramolecular π-stacking interactions within the coordination sphere of the ground-state complex. This inhibits flattening of the structure in the excited state; the flattening is associated with a change from tetrahedral to square-planar copper which accompanies oxidation of copper(I) to copper(II) in the MLCT excited state [14]. Many [Cu(POP)(6-Xbpy)]$^+$ and [Cu(POP)(6,6'-X$_2$bpy)]$^+$ cations exhibit face-to-face π-stacking between one phenyl ring of a PPh$_2$ unit and one arene ring of the POP backbone, while in [Cu(xantphos)(6-Xbpy)]$^+$ and [Cu(xantphos)(6,6'-X$_2$bpy)]$^+$ cations, face-to-face π-stacking between two phenyl rings of different PPh$_2$ units may be observed, see for example in reference [10]. However, since these π-stacking interactions are within a single ligand rather than between the PˆP and NˆN ligands, they may not be effective in preventing flattening of the coordination sphere. In terms of solid-state emission, inter-cation π-stacking might also be beneficial in militating against structural reorganization upon excitation. Examples of [Cu(PˆP)(NˆN)]$^+$ complexes in which the NˆN ligand contains an extended π-system and in which the single crystal structures reveal inter-cation π-stacking interactions include [Cu(xantphos)(NˆN)][PF$_6$] in which NˆN = 4,4'-bis(4-fluorophenyl)-6,6'-dimethyl-2,2'-bipyridine or 4,4'-bis(4-iodophenyl)-6,6'-dimethyl-2,2'-bipyridine. Interestingly, these two compounds also exhibit intra-cation π-stacking between the PˆP and NˆN ligands [15]. We were therefore motivated to investigate the structural features of a series of compounds in which intra- and/or inter-cation π-stacking in the solid state should be possible. We selected three NˆN ligands, **1**–**3** (Scheme 1) to combine with POP or xantphos in [Cu(PˆP)(NˆN)][PF$_6$] compounds.
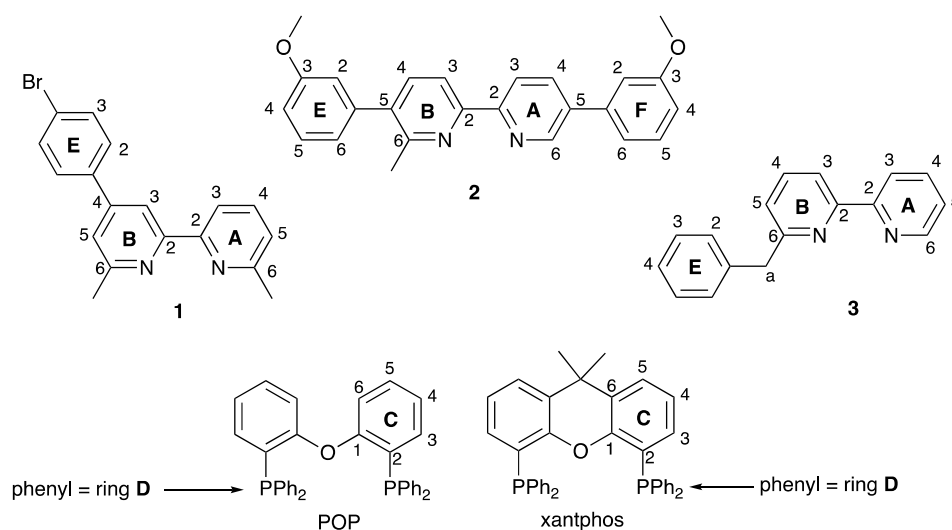
Scheme 1. Structures of ligands **1**–**3**, POP and xantphos with atom labelling used for NMR spectroscopic assignments. The phenyl rings of the PPh$_2$ units in POP and xantphos are labelled **D**.

2. Materials and Methods

2.1. General

^{1}H and ^{13}C{^{1}H} NMR spectra were recorded on a Bruker Avance III-500 spectrometer (Bruker BioSpin AG, Fällanden, Switzerland) at 298 K. The ^{1}H and ^{13}C NMR chemical shifts were referenced with respect to residual solvent peaks (δ TMS = 0). A Shimadzu UV-2600 spectrophotometer and a Shimadzu RF-5301PC spectrofluorometer, respectively (Shimadzu Schweiz GmbH, 4153 Aesch, Switzerland) were used to record solution absorption and emission spectra. A Shimadzu LCMS-2020 instrument (Shimadzu Schweiz GmbH, 4153 Aesch, Switzerland) was used to measure electrospray ionization (ESI) mass spectra (MeOH solutions). Quantum yields (CH_2Cl_2 solutions or powder samples) were determined using a Hamamatsu absolute photoluminescence quantum yield spectrometer C11347 Quantaurus-QY (Hamamatsu Photonics, 4500 Solothurn, Switzerland). Emission lifetimes and powder emission spectra were recorded with a Hamamatsu Compact Fluorescence lifetime Spectrometer C11367 Quantaurus-Tau (Hamamatsu Photonics, 4500 Solothurn, Switzerland) with an LED light source (λ_{exc} = 365 nm).

Cyclic voltammograms were recorded using a CH Instruments 900B potentiostat (HPLC grade CH_2Cl_2 solutions, ca. 10^{-5} mol dm^{-3}; 0.1 M [$^nBu_4N$][PF_6] as supporting electrolyte; scan rate of 100 mV s^{-1}). The working, reference and counter-electrodes were glassy carbon, a leakless Ag$^+$/AgCl (eDAQ ET069-1) and platinum wire, respectively. Referencing was against an internal Fc/Fc$^+$ couple.

6-Bromo-2,2′-bipyridine [16], compounds **1** [17], **2** [18] and **3** [19], and [Cu(MeCN)$_4$][PF$_6$] [20] were prepared as previously described. The yield of compound **3** was only 20% (24 mg) and for ease of handling, a stock solution in CH_2Cl_2 (0.01 M) was prepared. POP and xantphos were purchased from Fluorochem (Fluorochem Ltd., Hadfield, UK). Inert conditions were not required for the reactions.

2.2. [Cu(POP)(**1**)][PF$_6$]

[Cu(MeCN)$_4$][PF$_6$] (0.25 mmol, 93.1 mg) was dissolved in CH_2Cl_2 (30 mL) and POP (0.30 mmol, 160 mg) was added to the solution. The solution was stirred for 1.5 h at room temperature. Compound **1** (0.25 mmol, 84.7 mg) was added and the reaction mixture was again stirred for 1.5 h at room temperature. The reaction mixture was filtered, and the solvent was evaporated under reduced pressure. The crude product was washed with hexane (5 × 20 mL) and dried under vacuum, then recrystallized from CH_2Cl_2 and Et$_2$O. [Cu(POP)(**1**)][PF$_6$] (0.172 mmol, 186.4 mg, 68.6%) was obtained as a yellow solid. ^{1}H NMR (500 MHz, acetone-d_6) δ/ppm 8.50 (d, J = 1.6 Hz, 1H, H^{B3}), 8.47 (d, J = 8.0 Hz, 1H, H^{A3}), 8.05 (t, J = 7.9 Hz, 1H, H^{A4}), 7.91 (m, 2H, H^{E2}), 7.76 (m, 3H, H^{E3+B5}), 7.48–7.43 (m, 3H, H^{A5+C5}), 7.37-7.31 (m, 4H, H^{D4}), 7.31–7.27 (m, 4H, H^{C3+C4}), 7.23–7.19 (m, 8H, H^{D3}), 7.17–7.12 (m, 8H, H^{D2}), 7.07 (m, 2H, H^{C6}), 2.37 (s, 3H, H^{MeB}), 2.36 (s, 3H, H^{MeA}). ^{13}C{^{1}H} NMR (126 MHz, acetone-d_6) δ/ppm 160.1 (C^{B6}), 159.6 (C^{A6}), 159.1 (t, J_{PC} = 6 Hz, C^{C1}), 154.1 (C$^{A2/B2}$), 153.4 (C$^{A2/B2}$), 150.3 (C^{B4}), 139.9 (C^{A4}), 136.8 (C^{E1}), 134.5 (C$^{C3/C4}$), 133.9 (broad, C^{D2}), 133.3 (C^{C5}), 133.2 (C^{E3}), 132.8 (m, C^{D1}), 130.8 (broad, C^{D4}), 130.2 (C^{E2}), 129.6 (t, J_{PC} = 5 Hz, C^{D3}), 127.2 (C^{A5}), 126.2 (m, C$^{C3/C4+C2}$), 124.9 (C^{E4}), 124.5 (C^{B5}), 121.4 (C^{A3}), 121.0 (t, J_{PC} = 2 Hz, C^{C6}), 118.7 (C^{B3}), 27.0 (C^{MeA}), 26.9 (C^{MeB}). ^{31}P{^{1}H} NMR (202 MHz, acetone-d_6) δ/ppm −13.6 (broad, FWHM = 130 Hz), −144.2 (septet, J_{PF} = 708 Hz, [PF$_6$]$^-$). ESI-MS m/z 941.13 [M–PF$_6$]$^+$ (calc. 941.13), 601.13 [M–PF$_6$–**1**]$^+$ (base peak, calc. 601.09). UV-Vis (CH_2Cl_2, 2.5×10^{-5} mol dm^{-3}): λ/nm (ε/dm^3 mol^{-1} cm^{-1}) 272 (42,700), 307sh (24,500), 320sh (17,400), 385 (4,100). Found C 58.13, H 4.07, N 2.44%; $C_{54}H_{43}BrCuF_6N_2OP_3 \cdot 0.5CH_2Cl_2$ requires C 58.21, H 3.91, N 2.47%.

2.3. [Cu(xantphos)(**1**)][PF$_6$]

[Cu(MeCN)$_4$][PF$_6$] (0.25 mmol, 93.0 mg) was dissolved in CH_2Cl_2 (15 mL). **1** (0.25 mmol, 84.7 mg) and xantphos (0.25 mmol, 145 mg) were dissolved in CH_2Cl_2 (15 mL) in a separate flask and this solution was added to the solution of [Cu(MeCN)$_4$][PF$_6$]. The reaction mixture was stirred for 1.5 h at room temperature. The solution was then filtered, and the solvent was evaporated under reduced pressure. The crude product was washed with hexane (5 × 20 mL) and dried under vacuum, then

recrystallized from CH_2Cl_2 and Et_2O. [Cu(xantphos)(**1**)][PF_6] (0.164 mmol, 184.9 mg, 65.7%) was obtained as a yellow solid. ^1H NMR (500 MHz, acetone-d_6) δ/ppm 8.42 (d, J = 1.8 Hz, 1H, H^{B3}), 8.41 (d, J = 7.8 Hz, 1H, H^{A3}), 8.00 (t, J = 7.8 Hz, 1H, H^{A4}), 7.88 (m, 2H, H^{E2}), 7.84 (dd, J = 7.8, 1.4 Hz, 2H, H^{C5}), 7.75 (m, 2H, H^{E3}), 7.72 (d, J = 1.8 Hz, 1H, H^{B5}), 7.44–7.38 (overlapping m, 5H, H$^{A5+D4+D'4}$), 7.34–7.30 (dd, J = 7.8, 7.8 Hz, 2H, H^{C4}), 7.27–7.16 (overlapping m, 16H, H$^{D2+D'2+D3+D'3}$), 6.98 (m, 2H, H^{C3}), 2.23 (s, 3H, H^{MeB}), 2.15 (s, 3H, H^{MeA}), 1.77 (s, 3H, H$^{Me-xantphos}$), 1.75 (s, 3H, H$^{Me-xantphos}$). $^{13}C\{^1H\}$ NMR (126 MHz, acetone-d_6) δ/ppm 159.6 (C^{B6}), 159.2 (C^{A6}), 155.9 (t, J_{PC} = 6 Hz, C^{C1}), 153.8 (C$^{A2/B2}$), 153.2 (C$^{A2/B2}$), 150.3 (C^{B4}), 139.8 (C^{A4}), 136.7 (C^{E1}), 134.8 (t, J_{PC} = 2 Hz, C^{C6}), 134.1 and 134.0 (overlapping t, J_{PC} = 8 Hz, C$^{D2+D'2}$), 133.2 (C^{E3}), 132.5 and 132.4 (overlapping t, J_{PC} = 15 Hz, C$^{D1+D'1}$), 131.1 (C^{C3}), 131.05 (C$^{D4/D'4}$), 131.0 (C$^{D4/D'4}$), 130.2 (C^{E2}), 129.75 and 129.7 (overlapping t, J_{PC} = 5 Hz, C$^{D3+D'3}$), 128.7 (C^{C5}), 126.8 (C^{A5}), 126.4 (t, J_{PC} = 2 Hz, C^{C4}), 124.9 (C^{E4}), 124.0 (C^{B5}), 122.6 (t, J_{PC} = 14 Hz, C^{C2}), 121.4 (C^{A3}), 118.7 (C^{B3}), 36.9 (C$^{xantphos-\ bridge}$), 28.8 (C$^{Me-xantphos}$), 28.6 (C$^{Me-xantphos}$), 27.1 (C^{MeB}), 27.0 (C^{MeA}). $^{31}P\{^1H\}$ NMR (202 MHz, acetone-d_6) δ/ppm −13.6 (broad, FWHM = 160 Hz), −144.2 (septet, J_{PF} = 708 Hz, [PF_6]$^-$). ESI-MS m/z 981.16 [M–PF_6]$^+$ (base peak, calc. 981.16), 641.14 [M–PF_6–**1**]$^+$ (calc. 641.12). UV-Vis (CH_2Cl_2, 2.5×10^{-5} mol dm^{-3}): λ/nm (ε/dm^3 mol^{-1} cm^{-1}) 274 (45,200), 251sh (38,300), 321sh (15,600), 385 (4,200). Found: C 61.23, H 4.32, N 2.44%; $C_{57}H_{47}BrCuF_6N_2OP_3$ requires C 60.78, H 4.21, N 2.49%.

2.4. [Cu(POP)(**2**)][PF$_6$]

[Cu(MeCN)$_4$][PF$_6$] (0.25 mmol, 93.2 mg) was dissolved in CH_2Cl_2 (30 mL) and POP (0.3 mmol, 162 mg) was added. After stirring for 1.5 h at room temperature, compound **2** (0.25 mmol, 95.6 mg) was added and the reaction mixture was stirred for another 1.5 h at room temperature. The mixture was filtered, and the solvent removed under reduced pressure. The crude product was washed with hexane (5 × 20 mL) and dried in vacuo, redissolved in CH_2Cl_2 and precipitated with Et_2O. [Cu(POP)(**2**)][PF$_6$] (0.172 mmol, 194.8 mg, 69.0%) was isolated as a yellow solid. ^1H-NMR (500 MHz, acetone-d_6) δ/ppm 8.64 (d, J = 8.3 Hz, 1H, H^{A3}), 8.58 (dd, J = 2.3, 0.8 Hz, 1H, H^{A6}), 8.53 (d, J = 8.1 Hz, 1H, H^{B3}), 8.36 (dd, J = 8.3, 2.3 Hz, 1H, H^{A4}), 7.97 (d, J = 8.1 Hz, 1H, H^{B4}), 7.46–7.39 (overlapping m, 4H, H$^{F5+E5+C5}$), 7.39–7.31 (overlapping m, 10H, H$^{D4/D'4+D3/D'3+D2/D'2}$), 7.28 (m, 2H, H$^{D4/D'4}$), 7.22–7.16 (m, 6H, H$^{D3/D'3+C6}$), 7.14 (td, J = 1.0, 7.5 Hz, 2H, H^{C4}), 7.04 (ddd, J = 8.3, 2.6, 0.9 Hz, 1H, H$^{E4/F4}$), 7.01 (ddd, J = 8.4, 2.6, 1.0 Hz, 1H, H$^{E4/F4}$), 6.97 (m, 4H, H$^{D2/D'2}$), 6.93 (m, 2H, H^{C3}), 6.88 (m, 1H, H$^{E2/F2}$), 6.84 (ddd, J = 7.7, 1.8, 0.9 Hz, 1H, H$^{E6/F6}$), 6.75 (ddd, J = 7.5, 1.6, 0.9 Hz, 1H, H$^{E6/F6}$), 6.70 (dd, J = 2.6, 1.6 Hz, 1H, H$^{E2/F2}$), 3.89 (s, 3H, H^{OMe}), 3.83 (s, 3H, H^{OMe}), 2.60 (s, 3H, H^{Me}). $^{13}C\{^1H\}$ NMR (126 MHz, acetone-d_6) δ/ppm 161.3 (C$^{E3/F3}$), 160.7 (C$^{E3/F3}$), 158.9 (t, J_{PC} = 6.0 Hz, C^{C1}), 156.8 (C^{B6}), 152.1 (C$^{A2/B2}$), 151.3 (C$^{A2/B2}$), 148.2 (C^{A6}), 140.5 (C$^{E1/F1}$), 140.4 (C^{B4}), 140.2 (C^{B5}), 138.7 (C^{A5}), 137.7 (C$^{E1/F1}$), 137.3 (C^{A4}), 135.0 (C^{C3}), 134.4 (t, J_{PC} = 8 Hz, C$^{D'2/D2}$), 133.4 (t, J_{PC} = 8 Hz, C$^{D'2/D2}$), 133.3 (C^{C5}), 131.9 (C$^{D1/D'1}$), 131.7 (C$^{D1/D'1}$), 131.3 (C$^{D'4/D4}$), 131.2 (C$^{E5/F5}$), 130.9 (C$^{D'4/D4}$), 130.7 (C$^{E5/F5}$), 129.9 (t, J_{PC} = 5 Hz, C$^{D'3/D3}$), 129.6 (t, J_{PC} = 5 Hz, C$^{D'3/D3}$), 126.2 (t, J_{PC} = 2 Hz, C^{C4}), 125.0 (t, J_{PC} = 15 Hz, C^{C2}), 123.5 (C^{A3}), 121.8 (C$^{E6/F6}$), 121.3 (t, J_{PC} = 2 Hz, C^{C6}), 121.25 (C^{B3}), 120.0 (C$^{E6/F6}$), 115.4 (C$^{E4/F4}$), 115.2 (C$^{E2/F2}$), 114.5 (C$^{E4/F4}$), 113.3 (C$^{E2/F2}$), 55.9 (C^{OMe}), 55.8 (C^{OMe}), 27.0 (C^{Me}). $^{31}P\{^1H\}$ NMR (202 MHz, acetone-d_6) δ/ppm −12.0 (broad, FWHM = 160 Hz), −144.2 (septet, J_{PF} = 708 Hz, [PF_6]$^-$). ESI-MS m/z 983.29 [M–PF_6]$^+$ (base peak, calc. 983.26), 601.12 [M–PF_6–**2**]$^+$ (calc. 601.09). UV-Vis (CH_2Cl_2, 2.5×10^{-5} mol dm^{-3}): λ/nm (ε/dm^3 mol^{-1} cm^{-1}) 274 (35,600), 332 (30,200), 395 (2,990). Found: C 64.84, H 4.67, N 2.34%; $C_{61}H_{50}CuF_6N_2O_3P_3$ requires C 64.86, H 4.46, N 2.48%.

2.5. [Cu(xantphos)(**2**)][PF$_6$]

Solid **2** (0.25 mmol, 95.6 mg) and xantphos (0.25 mmol, 144 mg) were dissolved in CH_2Cl_2 (15 mL) and this solution was added to a solution of [Cu(MeCN)$_4$][PF$_6$] (0.25 mmol, 93.3 mg) in CH_2Cl_2 (15 mL). The mixture was stirred for 1.5 h at room temperature, and was then filtered and the filtrate collected. The solvent was removed under reduced pressure. The crude product was washed with hexane (5 × 20 mL) and dried under vacuum, then recrystallized from CH_2Cl_2 and

Et_2O. [Cu(xantphos)(**2**)][PF_6] (0.169 mmol, 197.8 mg, 67.6%) was isolated as a yellow solid. ^1H NMR (500 MHz, acetone-d_6) δ/ppm 8.67 (d, *J* = 8.5 Hz, 1H, H^{A3}), 8.53 (d, *J* = 8.1 Hz, 1H, H^{B3}), 8.35 (dd, *J* = 8.4, 2.3 Hz, 1H, H^{A4}), 8.02 (d, *J* = 8.1 Hz, 1H, H^{B4}), 7.83 (dd, *J* = 7.8, 1.4 Hz, 2H, H^{C5}), 7.68 (d, *J* = 2.2 Hz, 1H, H^{A6}), 7.43–7.35 (m, 6H, H$^{E5+F5+D4/D'4}$), 7.28–7.21 (m, 16H, H$^{C4+D3+D'3+D2/D'2+D4/D'4}$), 7.05 (dd, *J* = 8.3, 2.5 Hz, 1H, H$^{E4/F4}$), 7.01 (dd, *J* = 8.3, 2.5 Hz, 1H, H$^{E4/F4}$), 6.96 (m, 4H, H$^{D2/D'2}$), 6.80 (dt, *J* = 7.6, 1.2 Hz, 1H, H$^{E6/F6}$), 6.78–6.71 (m, 4H, H$^{E2+F2+C3}$), 6.41 (m, 1H, H$^{E6/F6}$), 3.89 (s, 3H, H^{OMe}), 3.81 (s, 3H, H^{OMe}), 2.73 (s, 3H, H^{MeB}), 1.90 (s, 3H, H$^{Me-xantphos}$), 1.59 (s, 3H, H$^{Me-xantphos}$). $^{13}C\{^1H\}$ NMR (126 MHz, acetone-d_6) δ/ppm 161.3 (C$^{E3/F3}$), 160.8 (C$^{E3/F3}$), 156.5 (C^{B6}), 155.9 (t, J_{PC} = 6 Hz, C^{C1}), 152.2 (C$^{A2/B2}$), 150.9 (C$^{A2/B2}$), 146.9 (C^{A6}), 140.5 (C$^{B4/A5/B5}$), 140.4 (C$^{B4/A5/B5}$), 140.3 (C$^{B4/A5/B5}$), 138.9 (C$^{E1/F1}$), 138.0 (C^{A4}), 137.4 (C$^{E1/F1}$), 135.2 (t, J_{PC} = 2 Hz, C^{C6}), 134.0 (t, J_{PC} = 8 Hz, C$^{D2/D'2}$), 133.5 (t, J_{PC} = 8 Hz, C$^{D2/D'2}$), 132.4 and 132.2 (overlapping t, J_{PC} = 18 Hz, C$^{D1+D'1}$), 131.6 (C^{C3}), 131.3 (C$^{D4+D'4}$), 130.9 (C$^{E5/F5}$), 130.7 (C$^{E5/F5}$), 129.9 and 129.8 (overlapping t, J_{PC} = 5 Hz, C$^{D3+D'3}$), 128.7 (C^{C5}), 126.4 (t, *J* = 2 Hz, C^{C4}), 123.9 (C^{A3}), 121.8 (C$^{E6/F6}$), 121.4 (C^{B3}), 121.0 (t, J_{PC} = 13 Hz, C^{C2}), 119.8 (C$^{E6/F6}$), 115.4 (C$^{E2/F2}$), 114.9 (C$^{E4/F4}$), 114.5 (C$^{E4/F4}$), 113.9 (C$^{E2/F2}$), 55.8 (C^{OMe}), 55.70 (C^{OMe}), 37.03 (C$^{xantphos-bridge}$), 30.8 (C$^{Me-xantphos}$), 27.3 (C^{MeB}), 25.2 (C$^{Me-xantphos}$). $^{31}P\{^1H\}$ NMR (202 MHz, acetone-d_6) δ/ppm −12.0 (broad, FWHM = 170 Hz), −144.2 (septet, J_{PF} = 708 Hz, [PF_6]$^-$). ESI-MS *m/z* 1023.30 [M–PF_6]$^+$ (base peak, calc. 1023.29), 641.14 [M–PF_6–**2**]$^+$ (calc. 641.12). UV-Vis (CH$_2$Cl$_2$, 2.5 × 10^{-5} mol dm^{-3}): λ/nm (ε/dm^3 mol^{-1} cm^{-1}) 277 (41,500), 333 (26,200), 395 (2,910). Found: C 65.61, H 4.81, N 2.35%; C$_{64}$H$_{54}$CuF$_6$N$_2$O$_3$P$_3$ requires C 65.72, H 4.65, N 2.40%.

2.6. [Cu(POP)(**3**)][PF$_6$]

POP (0.054 mmol, 29.1 mg) was added to a CH$_2$Cl$_2$ (15 mL) solution of [Cu(MeCN)$_4$][PF$_6$] (0.0494 mmol, 18.4 mg). The mixture was stirred for 1.5 h at room temperature and then **3** (0.0491 mmol, 0.01 M in CH$_2$Cl$_2$, 5 mL) was added and the reaction mixture was stirred again for 1.5 h. After filtration, the solvent was evaporated from the filtrate under reduced pressure. The crude product was washed with Et$_2$O (10 × 20 mL) and dried under vacuum. The solid product was crystallized from CH$_2$Cl$_2$ layered with Et$_2$O to obtain [Cu(POP)(**3**)][PF$_6$] (0.0008 mmol, 0.8 mg, 1.6%) as a yellow solid. ^1H NMR (500 MHz, acetone-d_6) δ/ppm 8.74 (m, 1H, H^{A6}), 8.61 (d, *J* = 8.2 Hz, 1H, H^{A3}), 8.53 (d, *J* = 7.9 Hz, 1H, H^{B3}), 8.17–8.09 (m, 2H, H^{A4+B4}), 7.49–7.36 (m, 8H, H$^{A5+E4+C5+D4+D'4}$), 7.35–7.25 (m, 8H, H$^{D3+D'3}$), 7.21–7.10 (m, 10H, H$^{E3+C4+C6+D2/D'2}$), 7.10–7.03 (m, 5H, H$^{B5+D2/D'2}$), 6.87 (m, 2H, H^{C3}), 6.50 (m, 2H, H^{E2}), 4.11 (s, 2H, H^a). $^{13}C\{^1H\}$ NMR (126 MHz, acetone-d_6) δ/ppm 162.1 (C^{B6}), 158.2 (C^{C1}), 152.0 (C^{A2+B2}), 149.7 (C^{A6}), 139.4 (C^{A4+B4}), 137.5 (C^{E1}), 134.2 (C^{C3}), 133.3 (C$^{D2/D'2}$), 132.9 (C$^{D2/D'2}$), 132.5 (C^{C5}), 131.4 (C$^{D1+D'1}$), 130.2 (C$^{D4+D'4+E4}$), 129.2 (C^{E2}), 129.0 (C$^{D3+D'3}$), 127.0 (C^{C2}), 125.9 (C^{A5}), 125.5 (C^{B5}), 125.2 (C^{C4+E3}), 123.2 (C^{A3}), 120.6 (C^{C6}), 120.2 (C^{B3}), 46.4 (C^a). $^{31}P\{^1H\}$ NMR (202 MHz, acetone-d_6) δ/ppm −13 (broad, FWHM = 300 Hz), −144.2 (septet, J_{PF} = 708 Hz, [PF$_6$]$^-$). ESI MS *m/z* 847.13 [M–PF$_6$]$^+$ (base peak, calc: 847.21), 601.12 [M–PF$_6$–**3**]$^+$ (calc. 601.13). Insufficient material for elemental analysis.

2.7. [Cu(xantphos)(**3**)][PF$_6$]

Compound **3** (0.0491 mmol, 0.01 M in CH$_2$Cl$_2$, 5 mL,) and xantphos (0.0491 mmol, 28.4 mg) were dissolved in CH$_2$Cl$_2$ (8 mL) and this solution was added to a CH$_2$Cl$_2$ (8 mL) solution of [Cu(MeCN)$_4$][PF$_6$] (0.0491 mmol, 18.3 mg). The reaction mixture was stirred for 1.5 h at room temperature and was then filtered. The solvent was removed from the filtrate under reduced pressure. The crude product was washed with Et$_2$O (5 × 20 mL) and dried under vacuum. The solid was dissolved in CH$_2$Cl$_2$ and was crystallized by layering with Et$_2$O. [Cu(xantphos)(**3**)][PF$_6$] (0.0013 mmol, 1.4 mg, 2.8%) was isolated as a yellow solid. ^1H NMR (500 MHz, acetone-d_6) δ/ppm 8.80 (br, 1H, H^{A6}) 8.61 (d, *J* = 8.2 Hz, 1H, H^{A3}), 8.54 (d, *J* = 7.9 Hz, 1H, H^{B3}), 8.18–8.08 (overlapping m, 2H, H^{A4+B4}), 7.64 (dd, *J* = 7.9, 1.6 Hz, 2H, H^{C5}), 7.58 (m, 1H, H^{A5}), 7.41–7.31 (overlapping m, 4H, H$^{D4+D'4}$), 7.28–7.19 (overlapping m, 10H, H$^{C4+D3/D'3+D2/D'2}$), 7.18–7.11 (overlapping m, 5H, H$^{E4+D3/D'3}$), 7.07–6.99 (overlapping m, 3H, H^{B5+E3}), 6.91–6.84 (m, 4H, H$^{D2/D'2}$), 6.63 (m, 2H, H^{C3}), 6.30 (m, 2H, H^{E2}), 3.61 (s,

2H, H^a), 1.56 (s, 6H, H$^{\text{Me-xantphos}}$). ^{13}C{^{1}H} NMR (126 MHz, acetone) δ/ppm 162.8 (C^{B6}), 156.0 (C^{C1}), 152.9 (C^{A2+B2}), 140.4 (C$^{A4/B4}$), 140.1 (C$^{A4/B4}$), 137.4 (C^{E1}), 135.0 (C^{C6}), 134.1 (C$^{D2/D'2}$), 133.3 (C$^{D2/D'2}$), 131.5 (C$^{D1+D'1}$), 131.3 (C^{C3}), 130.7 (C$^{D4+D'4}$), 129.9 (C$^{D3/D'3}$), 129.8 (C$^{D3/D'3}$), 129.5 (C^{E2}), 129.3 (C^{E3}), 128.7 (C^{C5}), 127.6 (C^{E4}), 127.2 (C^{A5}), 126.1 (C^{C4}), 125.8 (C^{B5}), 123.7 (C^{A3}), 121.6 (C^{C2}), 121.5 (C^{B3}), 47.2 (C^a), 36.9 (C$^{\text{xantphos-bridge}}$), 31.1 (C$^{\text{Me-xantphos}}$), 24.8 (C$^{\text{Me-xantphos}}$), signal for C^{A6} not observed. ^{31}P{^{1}H} NMR (202 MHz, acetone-d_6) δ/ppm −12.8 (broad, FWHM = 300 Hz), −144.3 (septet, J_{PF} = 708 Hz, [PF$_6$]$^-$). ESI-MS *m/z* 887.21 [M–PF$_6$]$^+$ (base peak, calc. 887.24), 640.88 [M–PF$_6$–**3**]$^+$ (calc. 641.12). Insufficent material for elemental analysis.

2.8. Crystallography

Single crystal data were collected on a Bruker APEX-II diffractometer (CuKα radiation) with data reduction, solution and refinement using the programs APEX [21], ShelXT [22], Olex2 [23] and ShelXL v. 2014/7 [24]. Structure analysis including the ORTEP-style diagrams used Mercury CSD v. 4.1.2 [25,26].

2.9. [Cu(xantphos)(**1**)][PF$_6$]·CH$_2$Cl$_2$

C$_{58}$H$_{49}$BrCl$_2$CuF$_6$N$_2$OP$_3$, M_r = 1211.25, yellow plate, triclinic, space group P–1, a = 12.4425(14), b = 14.0675(15), c = 17.4500(19) Å, α = 111.123(3), β = 102.141(3), γ = 103.614(3), V = 2618.2(5) Å^3, D_c = 1.536 g cm^{-3}, T = 130 K, Z = 2, Z' = 1, μ(CuKα) = 3.840 mm^{-1}. Total 33672 reflections, 9336 unique (R_{int} = 0.0276). Refinement of 9219 reflections (671 parameters) with $I > 2\sigma(I)$ converged at final R_1 = 0.0256 (R_1 all data = 0.0259), wR_2 = 0.0676 (wR_2 all data = 0.0679), gof = 1.035. CCDC 1963589.

2.10. [Cu(xantphos)(**2**)][PF$_6$]·CH$_2$Cl$_2$

C$_{65}$H$_{56}$Cl$_2$CuF$_6$N$_2$O$_3$P$_3$, M_r = 1254.46, yellow block, triclinic, space group P–1, a = 11.7930(9), b = 14.3983(10), c = 16.9872(12) Å, α = 84.628(2), β = 89.728(2), γ = 88.073(2), V = 2870.1(4) Å^3, D_c = 1.452 g cm^{-3}, T = 130 K, Z = 2, Z' = 1, μ(CuKα) = 2.768 mm^{-1}. Total 22437 reflections, 10140 unique (R_{int} = 0.0563). Refinement of 9282 reflections (744 parameters) with $I > 2\sigma(I)$ converged at final R_1 = 0.0500 (R_1 all data = 0.0546), wR_2 = 0.1399 (wR_2 all data = 0.1439), gof = 1.036. CCDC 1963587.

2.11. [Cu(POP)(**3**)][PF$_6$]·0.5H$_2$O

C$_{53}$H$_{43}$CuF$_6$N$_2$O$_{1.5}$P$_3$, M_r = 1002.34, yellow needle, monoclinic, space group $P2_1/n$, a = 9.8270(6), b = 28.8706(18), c = 16.3488(12) Å, β = 102.702(3), V = 4524.8(5) Å^3, D_c = 1.471 g cm^{-3}, T = 130 K, Z = 4, Z' = 1, μ(CuKα) = 2.271 mm^{-1}. Total 39894 reflections, 8262 unique (R_{int} = 0.0423). Refinement of 7426 reflections (607 parameters) with $I > 2\sigma(I)$ converged at final R_1 = 0.0485 (R_1 all data = 0.0533), wR_2 = 0.1226 (wR_2 all data = 0.1275), gof = 1.122. CCDC 1963588.

3. Results and Discussion

3.1. Synthesis and Mass Spectrometric and NMR Spectroscopic Characterization of the Copper(I) Compounds

As previously discussed [9–11], the synthetic route to [Cu(POP)(N^N)][PF$_6$] and [Cu(xantphos)(N^N)][PF$_6$] compounds differs because of competing equilibria in solution leading to homoleptic [Cu(N^N)$_2$]$^+$ and [Cu(P^P)$_2$]$^+$ complexes. For the POP-containing compounds, [Cu(MeCN)$_4$][PF$_6$] was first treated with POP in CH$_2$Cl$_2$, and after about 1.5 h at room temperature, ligand **1**, **2** or **3** was added. For the preparation of [Cu(xantphos)(N^N)][PF$_6$], a CH$_2$Cl$_2$ solution of the N^N ligand and xantphos was added to a solution of [Cu(MeCN)$_4$][PF$_6$] in CH$_2$Cl$_2$ at room temperature. The products were isolated as yellow solids and, after recrystallization, the compounds containing ligands **1** or **2** were isolated in yields of between 65.7% and 69.0%. Yields of recrystallized [Cu(POP)(**3**)][PF$_6$] and [Cu(xantphos)(**3**)][PF$_6$] were very low (<3%).

Figures S1–S6 (see Supporting Information) display the electrospray mass spectra of the [Cu(POP)(N^N)][PF$_6$] and [Cu(xantphos)(N^N)][PF$_6$] compounds with N^N = **1**, **2** or **3**. All show peaks arising from the [M–PF$_6$]$^+$ ion in addition to the [M–PF$_6$–**1**]$^+$, [M–PF$_6$–**2**]$^+$ or [M–PF$_6$–**3**]$^+$ ion.

For compounds containing **1**, $[M–PF_6–\mathbf{1}]^+$ gives rise to the base peak, whereas for ligands **2** and **3**, the dominant peak arises from the $[M–PF_6]^+$ ion.

The ^1H, $^{13}C\{^1H\}$ and $^{31}P\{^1H\}$ NMR spectra were recorded in acetone-d_6, and COSY, NOESY, HMQC and HMBC experiments were used to assign the ^1H and ^{13}C NMR resonances. For $[Cu(POP)(\mathbf{3})][PF_6]$ and $[Cu(xantphos)(\mathbf{3})][PF_6]$, well-resolved 1D $^{13}C\{^1H\}$ NMR spectra were not obtained and the ^{13}C chemical shifts were identified by using the HMQC and HMBC spectra. NMR spectra are shown in Figures S7–S27 (see Supporting Information). The $^{31}P\{^1H\}$ NMR spectrum of each of the six compounds exhibits one broadened signal in addition to the septet for the $[PF_6]^-$ ion (Figure S28, see Supporting Information).

In each N^N ligand, the pyridine rings are non-equivalent on the NMR spectroscopic time scale at room temperature. In **1**, this is a consequence of the 4-(4-bromophenyl)-substituent which is remote from the copper(I) coordination sphere. In **2** and **3**, the asymmetry of the bpy domain is due to the presence of the 6-methyl (in **2**) or 6-benzyl (in **3**) substituent which is spatially close to the phenyl rings of the POP or xantphos ligands. Dynamic processes affecting the PPh_2 units in $[Cu(POP)(N^N)]^+$ involve rotation of the phenyl groups around the P–C bonds and conformational changes of the Cu(POP) 8-membered chelate ring. The coordinated xantphos ligand is significantly less flexible than POP. Dynamic processes involving the xantphos in $[Cu(xantphos)(N^N)]^+$ include rotation of the phenyl rings and inversion of the xanthene 'bowl'. These differences are nicely illustrated by comparing the aromatic regions of the room temperature ^1H NMR spectra of $[Cu(POP)(\mathbf{1})][PF_6]$ and $[Cu(xantphos)(\mathbf{1})][PF_6]$ (Figure 1a,b) and the $^{13}C\{^1H\}$ NMR spectra (Figure 2). The signals for the phenyl protons H^{D2} and H^{D3} (ortho and meta positions) split into two sets on going from $[Cu(POP)(\mathbf{1})][PF_6]$ (Figure 1a) to $[Cu(xantphos)(\mathbf{1})][PF_6]$ (Figure 1b). In the $^{13}C\{^1H\}$ NMR spectra, two sets of signals for C^{D1}, C^{D2}, C^{D3} and C^{D4} are observed for $[Cu(xantphos)(\mathbf{1})][PF_6]$ (Figure 2b) corresponding, respectively, to the two phenyl rings pointing towards and away from the bpy unit. In $[Cu(POP)(\mathbf{1})][PF_6]$, the broadened signals for C^{D2} and C^{D4} (Figure 2a) indicate slow exchange of the 'up' and 'down' sets of phenyl rings on the NMR timescale at 298 K, consistent with the greater flexibility of coordinated POP versus xantphos ligands. The fact that the signal for C^{D3} is sharp presumably reflects a small chemical shift difference between resonances for C^{D3} and $C^{D'3}$ in the 'up' and 'down' positions in $[Cu(POP)(\mathbf{1})][PF_6]$. This is indeed observed in $[Cu(xantphos)(\mathbf{1})][PF_6]$ in Figure 2b. The alkyl regions of the ^1H NMR spectra of $[Cu(POP)(\mathbf{1})][PF_6]$ and $[Cu(xantphos)(\mathbf{1})][PF_6]$ are shown in Figure 1c,d. Apart from the appearance of the signals for the xantphos methyl groups, the chemical environments of the bpy 6- and 6'-methyl groups change significantly. This reflects the location of one methyl group over the xanthene 'bowl' and will be discussed further in Section 3.2.
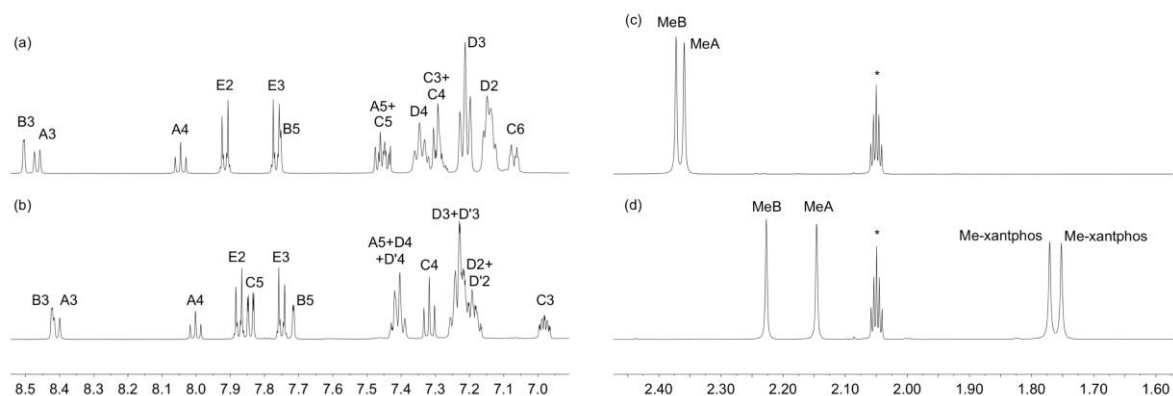

Figure 1. Comparison of the ^1H NMR spectra of $[Cu(POP)(\mathbf{1})][PF_6]$ and $[Cu(xantphos)(\mathbf{1})][PF_6]$ (500 MHz, acetone-d_6, 298 K). (**a**) Aromatic region of $[Cu(POP)(\mathbf{1})][PF_6]$. (**b**) Aromatic region of $[Cu(xantphos)(\mathbf{1})][PF_6]$. (**c**) Alkyl region of $[Cu(POP)(\mathbf{1})][PF_6]$. (**d**) Alkyl region of $[Cu(xantphos)(\mathbf{1})][PF_6]$. in (c) and (d): * = residual acetone-d_5. See Scheme 1 for atom labelling. Scales: δ/ppm.
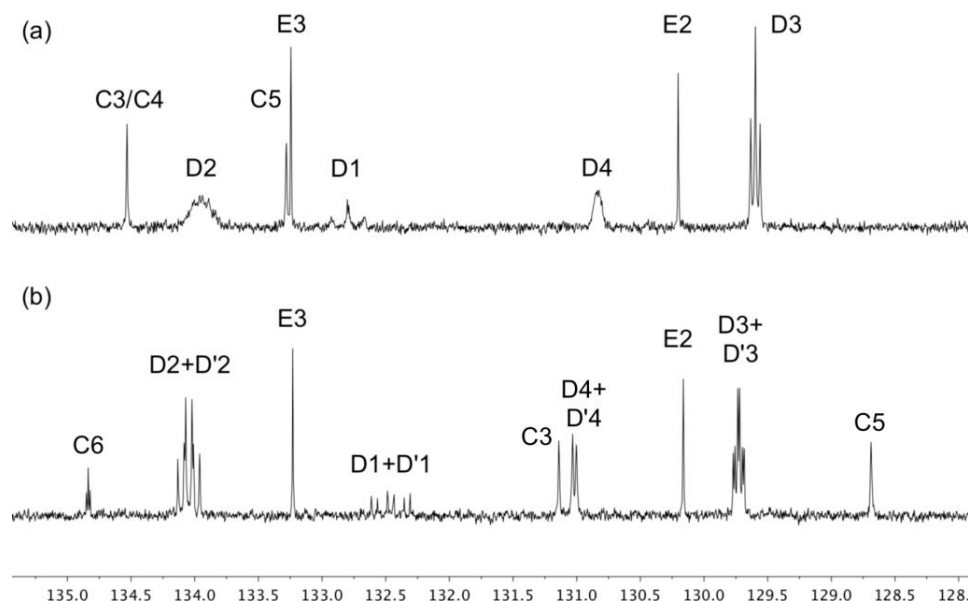
Figure 2. Comparison of parts of the $^{13}C\{^1H\}$ NMR spectra (126 MHz, acetone-d_6, 298 K) of (**a**) [Cu(POP)(**1**)][PF$_6$] and (**b**) [Cu(xantphos)(**1**)][PF$_6$]. See Scheme 1 for atom labelling. Scale: δ/ppm.

Compared to **1**, ligands **2** and **3** are sterically more demanding when we consider the immediate environment of the copper centre. Figure 3 shows part of the $^{13}C\{^1H\}$ NMR spectrum of [Cu(POP)(**2**)][PF$_6$] in which signals assigned to two sets of PPh$_2$ phenyl rings are observed. This is also detected in the HMQC spectrum of [Cu(POP)(**3**)][PF$_6$] (Figure S24). These data are consistent with the dynamic behaviour of the backbone of the POP ligand (concomitant with conformational changes of the Cu(POP) chelate ring) being slower on the NMR timescale at 298 K than in [Cu(POP)(**1**)][PF$_6$].
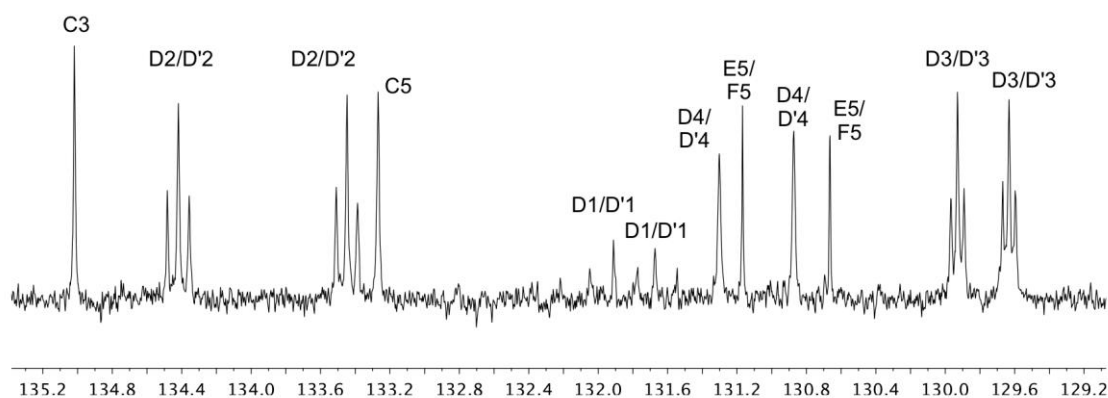
Figure 3. Part of the $^{13}C\{^1H\}$ NMR spectra (126 MHz, acetone-d_6, 298 K) of [Cu(POP)(**2**)][PF$_6$]. See Scheme 1 for atom labelling. Scale: δ/ppm.

3.2. Crystal Structures of [Cu(xantphos)(1)][PF$_6$]·CH$_2$Cl$_2$, [Cu(xantphos)(2)][PF$_6$]·CH$_2$Cl$_2$ and [Cu(POP)(3)][PF$_6$]·0.5H$_2$O

Single crystals of [Cu(xantphos)(**1**)][PF$_6$]·CH$_2$Cl$_2$ and [Cu(POP)(**3**)][PF$_6$]·0.5H$_2$O were obtained by slow evaporation of CH$_2$Cl$_2$ solutions of the compounds, while X-ray quality crystals of [Cu(xantphos)(**2**)][PF$_6$]·CH$_2$Cl$_2$ grew from a CH$_2$Cl$_2$ solution layered with hexanes. The compounds with ligands **1** and **2** crystallize in the triclinic space group *P*–1 and [Cu(POP)(**3**)][PF$_6$]·0.5H$_2$O crystallizes in the monoclinic space group *P*2$_1$/*n*. The structures of the [Cu(xantphos)(**1**)]$^+$, [Cu(xantphos)(**2**)]$^+$ and [Cu(POP)(**3**)]$^+$ cations are shown in Figures 4–6, respectively, and selected bond parameters are given in the figure captions. In each [Cu(P^P)(N^N)]$^+$ cation, the copper atom is in a distorted tetrahedral environment and Table 1 compares the bond parameters for the coordination spheres. The distortion

away from an ideal tetrahedral geometry is significant and may be quantified using Houser's τ_4 parameter [27] which has values of 1.00 for T_d and 0.85 for C_{3v} symmetries. The values in Table 1 are consistent with distorted C_{3v} symmetries and a greater distortion for the xantphos-containing complexes, with one large P–Cu–N bond angle in each cation (see captions to Figures 3 and 4) being a contributing factor.
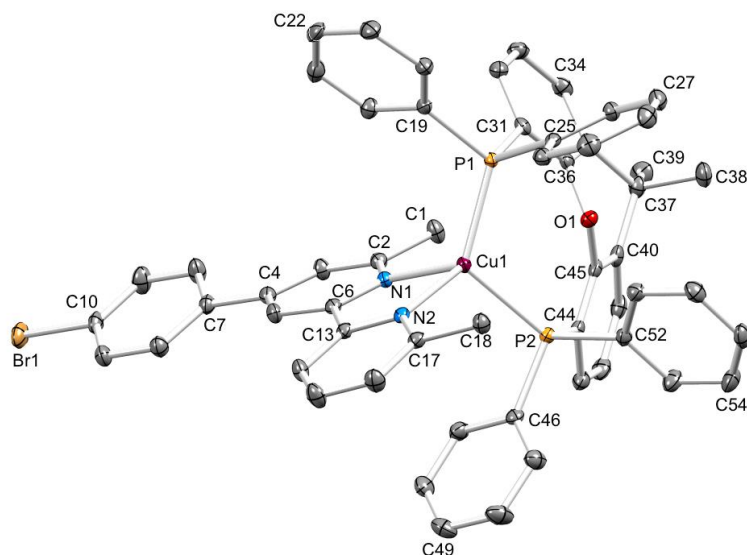

Figure 4. ORTEP-representation of the [Cu(xantphos)(**1**)]$^+$ cation in [Cu(xantphos)(**1**)][PF$_6$]·CH$_2$Cl$_2$. Ellipsoids are plotted at 50% probability level and H atoms are omitted for clarity. Selected bond parameters: Cu1–P1 = 2.2589(5), Cu1–P2 = 2.3038(5), Cu1–N1 = 2.1142(13), Cu1–N2 = 2.0796(13), O1–C36 = 1.3932(18), O1–C45 = 1.3946(19), Br1–C10 = 1.9039(16) Å; P1–Cu1–P2 = 116.050(17), N1–Cu1–P1 = 112.60(4), N1–Cu1–P2 = 113.19(4), N2–Cu1–P1 = 126.62(4), N2–Cu1–P2 = 103.97(4), N2–Cu1–N1 = 79.05(5), C36–O1–C45 = 114.09(12).
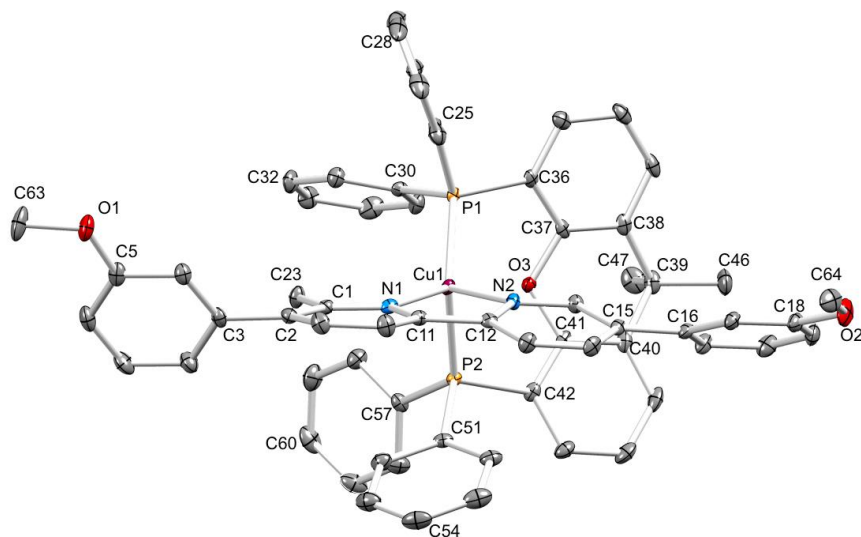

Figure 5. ORTEP-representation of the [Cu(xantphos)(**2**)]$^+$ cation in [Cu(xantphos)(**2**)][PF$_6$]·CH$_2$Cl$_2$. Ellipsoids are plotted at 50% probability level and H atoms are omitted for clarity. Selected bond parameters: Cu1–P1 = 2.2241(6), Cu1–P2 = 2.2729(6), Cu1–N2 = 2.0654(18), Cu1–N1 = 2.0693(18), O1–C5 = 1.367(3), O1–C63 = 1.432(3), O2–C18 = 1.367(3), O2–C64 = 1.426(3), O3–C37 = 1.388(3), O3–C41 = 1.380(2) Å; P1–Cu1–P2 = 120.05(2), N–Cu1–P1 = 116.33(5), N2–Cu1–P2 = 102.15(5), N2–Cu1–N1 = 79.45(7), N1–Cu1–P1 = 124.81(5), N1–Cu1–P2 = 105.28(5), C5–O1–C63 117.41(19), C18–O2–C64 = 117.31(19), C41–O3–C37 = 116.52(17).
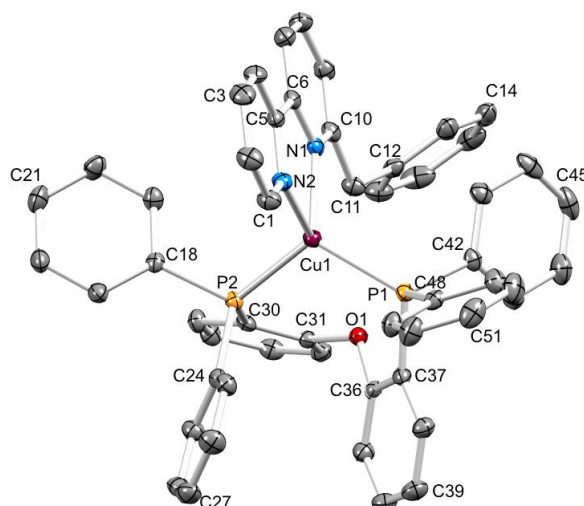
Figure 6. ORTEP-representation of the $[Cu(POP)(\mathbf{3})]^+$ cation in $[Cu(POP)(\mathbf{3})][PF_6]\cdot0.5\ H_2O$. Ellipsoids are plotted at 40% probability level for clarity, and H atoms are omitted. Selected bond parameters: Cu1–P2 = 2.2789(7), Cu1–P1 = 2.2662(7), Cu1–N2 = 2.060(2), Cu1–N1 = 2.127(2), O1–C36 = 1.388(3), O1–C31 = 1.399(3) Å; P1–Cu1–P2 = 112.83(3), N2–Cu1–P2 = 114.28(6), N2–Cu1–P1 = 115.64(6), N2–Cu1–N1 = 79.68(8), N1–Cu1–P2 = 111.24(6), N1–Cu1–P1 = 119.34(6), C36–O1–C31 = 119.64(19), C10–C11–C12 = 116.1(2).

Table 1. Comparison of the bond lengths and angles in the coordination sphere of each complex cation.

$[Cu(P\widehat{\ }P)(N\widehat{\ }N)]^+$ Cation	Cu–N/Å	Cu–P/Å	P–Cu–P/°	N–Cu–N/°	τ_4 [1]
$[Cu(xantphos)(\mathbf{1})]^+$	2.1142(13), 2.0796(13)	2.2589(5), 2.3038(5)	116.050(17)	79.05(5)	0.83
$[Cu(xantphos)(\mathbf{2})]^+$	2.0654(18), 2.0693(18)	2.2241(6), 2.2729(6)	120.05(2)	79.45(7)	0.82
$[Cu(POP)(\mathbf{3})]^+$	2.060(2), 2.127(2)	2.2789(7), 2.2662(7)	112.83(3)	79.68(8)	0.89

[1] τ_4 parameter, see reference [27].

The packing interactions in the three compounds illustrate both intra-cation and inter-cation π-contacts. In $[Cu(xantphos)(\mathbf{1})][PF_6]\cdot CH_2Cl_2$, the N^N and P^P ligands engage in a face-to-face π-stacking interaction involving the pyridine ring with N2 and the phenyl ring containing C46 (Figure 7a). The interaction is not optimal [28] since the angle between the ring planes is 22.6° and the centroid ... centroid distance is 3.95 Å. Nonetheless, it is interesting to note that a similar interaction occurs in $[Cu(xantphos)(N\widehat{\ }N)][PF_6]$ where N^N is 4,4′-bis(4-halophenyl)-6,6′-dimethyl-2,2′-bipyridine [15], symmetrical analogues of ligand **1**. The N^N and P^P ligands in $[Cu(xantphos)(\mathbf{2})][PF_6]\cdot CH_2Cl_2$ also interact through face-to-face π-stacking of a pyridine ring (with N1) and a PPh_2 phenyl ring (the ring containing C51). This is depicted in Figure 7b. Once again, the interaction is not optimal [28] with an angle between the ring planes of 29.1° and a centroid ... centroid distance of 4.14 Å. A search of the Cambridge Structural Database (CSD, v. 5.40 with February 2019 updates [29]) for {Cu(xantphos)(bpy)}-containing compounds (excluding {Cu(xantphos)(phen)}) revealed 33 entries of which only six contained N^N/P^P ligand π-stacking interactions, always face-to-face stacking of the bpy domain and a PPh_2 phenyl ring. These six structures have CSD refcodes EVADOW [15], EVADUC [15], EVAFEO [15], EVAFOY [15], VAWDUV [11] and VICREH [13]. In two other structures (CSD refcodes HIJQUP [30] and VANYUH [31]), inefficient bpy ... phenyl π-stacking occurs with angles between the least squares planes of the rings of 38.3° (HIJQUP) and 27.3° (VANYUH). In $[Cu(xantphos)(\mathbf{2})][PF_6]\cdot CH_2Cl_2$, there are also efficient inter-cation face-to-face π-contacts between ligands **2** (Figure 7c). These are between centrosymmetric pairs of

arene rings with C18 and C18^i (symmetry code i = $-x$, $1 - y$, $1 - z$) and centrosymmetric pairs of phenyl rings containing C25 and C25^{ii} (symmetry code ii = $-x$, $-y$, $2 - z$). In both motifs, the stacked rings are offset. For the first interaction, the distance between the ring planes is 3.53 Å and between the ring centroids is 3.93 Å, and for the second, the corresponding distances are 3.15 and 4.34 Å. The inter-cation embraces extend to produce infinite chains as shown in Figure 7c.
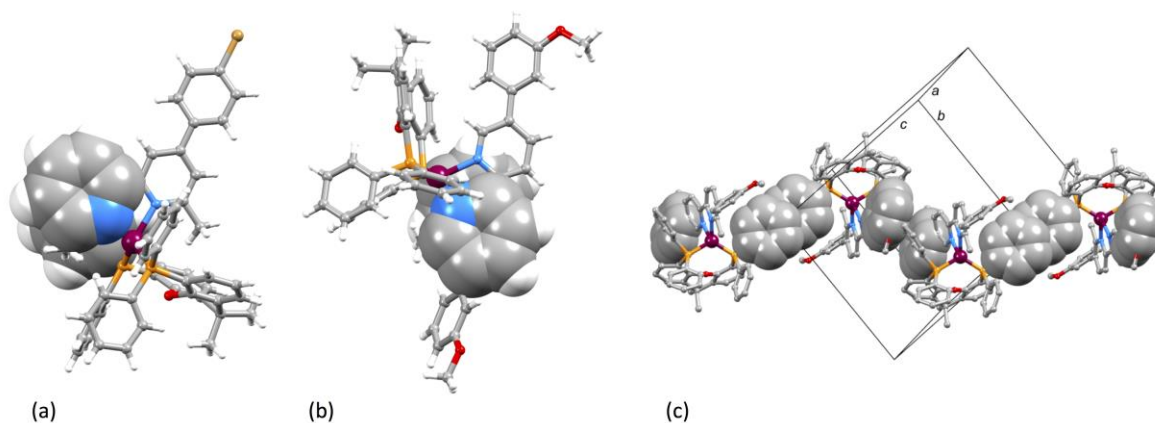

Figure 7. Intra-cation π-stacking in (**a**) [Cu(xantphos)(**1**)]$^+$ and (**b**) [Cu(xantphos)(**2**)]$^+$. (**c**) Inter-cation π-stacking interactions in [Cu(xantphos)(**2**)][PF$_6$]·CH$_2$Cl$_2$ extend to give infinite chains which run obliquely through the unit cell.

The introduction of the 6-benzyl substituent in ligand **3** allows the possibility of intra-cation π-stacking with an aryl ring of the POP or xantphos ligand. In the solid-state structure of [Cu(POP)(**3**)][PF$_6$], the benzyl unit faces towards the (C$_6$H$_4$)$_2$O-unit of the POP ligand but is not engaged in π-contacts, neither edge-to-face nor face-to-face. The only intra-cation π-stacking occurs between the aryl rings containing C24 and C36 (Figure 8a), but since the angle between the ring planes is 26.5° and the centroid . . . centroid distance is 4.15 Å, this interaction is not optimal. Centrosymmetric pairs of [Cu(POP)(**3**)]$^+$ cations engage in a combination of C–H . . . π (phenyl to bpy) and offset face-to-face (bpy . . . bpy) contacts (Figure 8b) which generate a motif which is reminiscent of the 'parallel quadruple aryl embrace' described by Dance et al. for [Ru(bpy)$_3$] [32]. The offset bpy . . . bpy interaction involves the rings containing N2 and N2^i (symmetry code i = $1 - x$, $1 - y$, $1 - z$) with an inter-plane separation of 3.50 Å and centroid . . . centroid distance of 3.93 Å, parameters that are consistent with an efficient interaction [28]. The C–H . . . π contacts involve C3–H3 and the phenyl ring containing C18^i with a C–H . . . centroid separation of 2.62 Å.
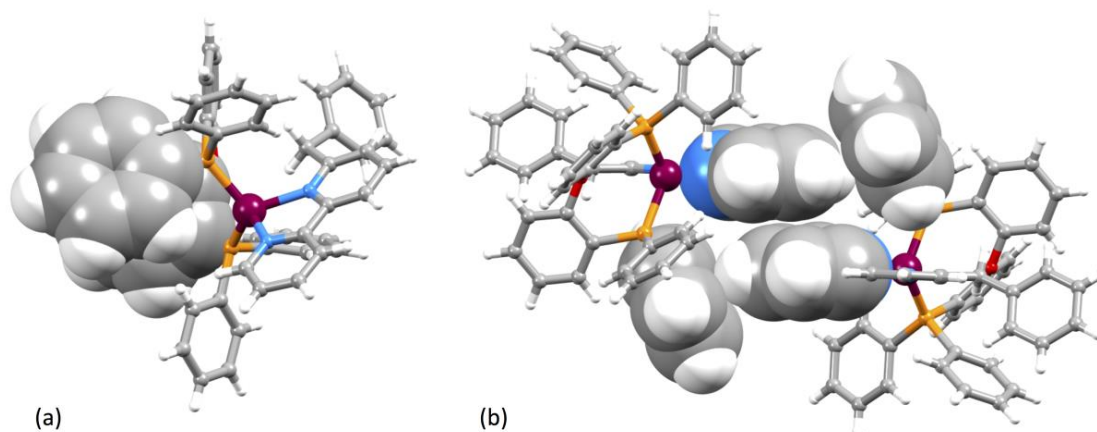

Figure 8. Packing motifs in [Cu(POP)(**3**)][PF$_6$]·0.5H$_2$O. (**a**) Intra-cation face-to-face π-stacking of one aryl ring of the POP backbone and one phenyl ring of a PPh$_2$ unit. (**b**) Inter-cation C–H . . . π (phenyl to bpy) and offset face-to-face (bpy . . . bpy) contacts.

3.3. Electrochemical and Photophysical Properties

The low yields of the copper(I) complexes containing ligand **3** precluded investigations of their electrochemical and photophysical properties. We focus, therefore, on the behaviour of [Cu(POP)(**1**)][PF$_6$], [Cu(xantphos)(**1**)][PF$_6$], [Cu(POP)(**2**)][PF$_6$], and [Cu(xantphos)(**2**)][PF$_6$]. Cyclic voltammograms of CH$_2$Cl$_2$ solutions of these compounds are shown in Figures S29–S32 (see Supporting Information) and Table 2 gives the potentials of the electrochemical processes. Each of [Cu(xantphos)(**1**)][PF$_6$], [Cu(POP)(**2**)][PF$_6$] and [Cu(xantphos)(**2**)][PF$_6$] undergoes a quasi-reversible oxidation process assigned to the Cu$^+$/Cu^{2+} redox couple. For [Cu(POP)(**1**)][PF$_6$], the process is irreversible; no well-defined reduction process is visible on the return wave (Figure S29). The oxidation potentials in Table 2 for the compounds containing ligand **2** compare to values of +0.69 V for [Cu(POP)(6-Mebpy)][PF$_6$] [8] and +0.85 V for [Cu(xantphos)(6-Mebpy)][PF$_6$] [13]. The oxidation potential of +0.87 V for [Cu(xantphos)(**1**)][PF$_6$] is similar to the +0.92 V observed for [Cu(xantphos)(**4**)][PF$_6$] where **4** is 4,4′-bis(4-bromophenyl)-6,6′-dimethyl-2,2′-bipyridine [15]. The irreversible process for [Cu(POP)(**1**)][PF$_6$] is consistent with the irreversible copper(I) oxidation observed for [Cu(xantphos)(**4**)][PF$_6$] [15]. [Cu(POP)(**1**)][PF$_6$] and [Cu(xantphos)(**1**)][PF$_6$] show only irreversible reduction processes (Table 2) while [Cu(POP)(**2**)][PF$_6$] and [Cu(xantphos)(**2**)][PF$_6$] show reversible reduction processes at −2.04 and −2.00 V, respectively.

Table 2. Cyclic voltammetric data for [Cu(P^P)(N^N)][PF$_6$] complexes referenced to internal Fc/Fc$^+$ = 0.0 V; CH$_2$Cl$_2$ solutions with [^{n}Bu$_4$N][PF$_6$] as supporting electrolyte and scan rate of 0.1 V s^{-1}.

Cation in [Cu(P^P)(N^N)][PF$_6$]	$E_{1/2}^{ox}$/V	$E_{pc} - E_{pa}$/mV	$E_{1/2}^{red}$/V	$E_{pc} - E_{pa}$/mV
[Cu(POP)(**1**)]$^+$	+0.92 [a]	-	−2.21, −2.11 [b]	-
[Cu(xantphos)(**1**)]$^+$	+0.87	80	−2.18, −2.10 [b]	-
[Cu(POP)(**2**)]$^+$	+0.81	100	−2.04	130
[Cu(xantphos)(**2**)]$^+$	+0.84	110	−2.00	130

[a] The value is for E_{pc}; the process is irreversible. [b] The values are for E_{pa}; each process is irreversible.

Table 3 and Figure 9 present the solution absorption spectroscopic data for the [Cu(POP)(N^N)][PF$_6$] and [Cu(xantphos)(N^N)][PF$_6$] complexes containing ligands **1** and **2**. The profiles of the spectra are strongly dependent upon the N^N ligand. The lowest energy absorptions are assigned to spin-allowed ligand-based transitions while the broad absorption band close to 400 nm arises from metal-to-ligand charge transfer (MLCT).
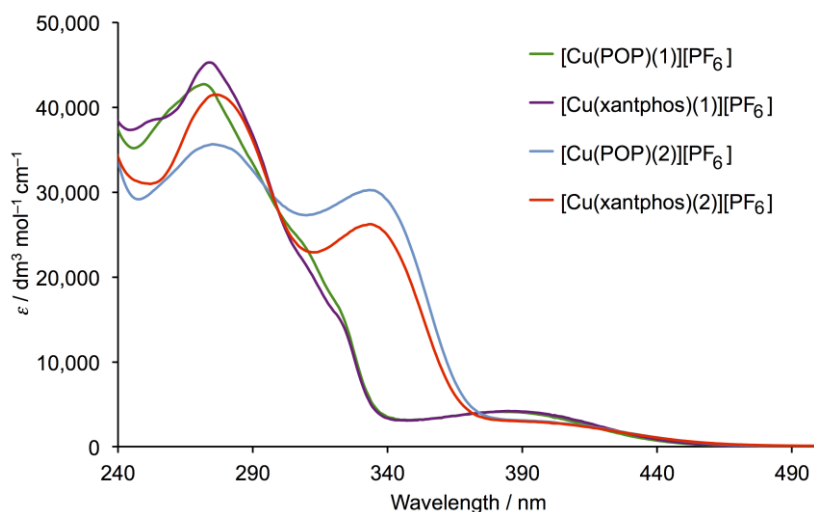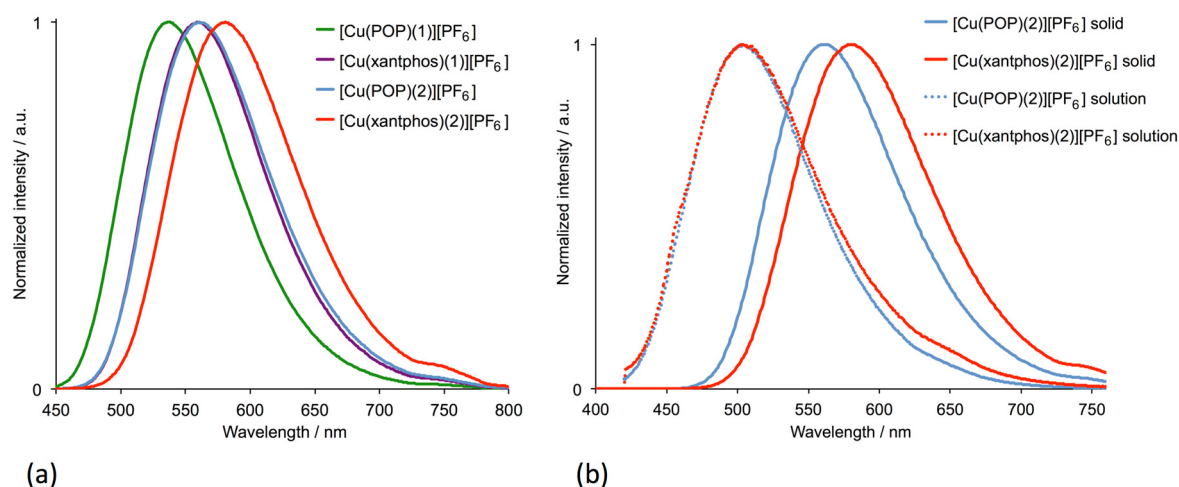

Figure 9. Solution absorption spectra of the [Cu(P^P)(N^N)][PF$_6$] complexes in CH$_2$Cl$_2$ (2.5×10^{-5} mol dm^{-3}).

Table 3. Solution absorption maxima for the [Cu(P^P)(N^N)][PF$_6$] complexes in CH$_2$Cl$_2$ (2.5×10^{-5} mol dm^{-3}).

Cation in [Cu(P^P)(N^N)][PF$_6$]	λ_{max}/nm (ε/dm^3 mol^{-1} cm^{-1})	
	Ligand-Based Absorptions	**MLCT**
[Cu(POP)(**1**)]$^+$	260 sh (40,000), 272 (42,600), 308 sh (24,100), 322 sh (16,300)	390 (4100)
[Cu(xantphos)(**1**)]$^+$	253 sh (38,500), 274 (45,200), 321 sh (15,100)	390 (4100)
[Cu(POP)(**2**)]$^+$	276 (35,500), 333 (30,200)	400 (2700)
[Cu(xantphos)(**2**)]$^+$	277 (41,450), 333 (26,200)	400 (2700)

The emission behavior of the compounds was investigated in CH$_2$Cl$_2$ solution (deaerated and non-deaerated) and for powdered samples, and data are summarized in Tables 4 and 5. The solid-state emission spectra are shown in Figure 10a. When excited at 365 nm, solutions of [Cu(POP)(**2**)][PF$_6$] and [Cu(xantphos)(**2**)][PF$_6$] both emit at 500 nm, and a red-shift is observed on going from [Cu(P^P)(**2**)][PF$_6$] to [Cu(P^P)(**1**)][PF$_6$] (Table 4). In deaearated solutions, the compounds show PLQY values in the range of 10%–20%. The emission maxima of [Cu(POP)(**1**)][PF$_6$] and [Cu(xantphos)(**1**)][PF$_6$] are blue-shifted on going from solution to the powdered samples, and this follows the typical trend [9,12]. However, for the compounds containing ligand **2**, a red-shift is observed from solution to solid (Figure 10b) and this is probably associated with the extensive intermolecular π-stacking between ligands **2** that is confirmed in the crystal structure of [Cu(xantphos)(**2**)][PF$_6$]·CH$_2$Cl$_2$. Where a comparable red-shift has been observed for other emissive metal coordination compounds, strong intermolecular interactions (e.g., in thin films) have been suggested as the cause [4]. The PLQY is significantly enhanced on going from solution to the solid state (Table 5) with the compounds containing ligand **1** having the highest values.

(a)   (b)

Figure 10. (**a**) Normalized emission spectra of powdered samples of the [Cu(P^P)(N^N)][PF$_6$] complexes (λ_{exc} = 365 nm). (**b**) Normalized emission spectra of solution (CH$_2$Cl$_2$, 2.5×10^{-6} mol dm^{-3}) and powdered samples of the [Cu(P^P)(**2**)][PF$_6$] complexes (λ_{exc} = 365 nm).

Table 4. Emission maxima and photoluminescence quantum yield (PLQY) values for [Cu(P^P)(N^N)][PF$_6$] complexes in CH$_2$Cl$_2$ solutions.

Cation in [Cu(P^P)(N^N)][PF$_6$]	λ_{exc}/nm	λ_{em}/nm	PLQY [a] (Non-Deaerated)/%	PLQY [a] (Deaerated)/%
[Cu(POP)(**1**)]$^+$	365	575	2	20
[Cu(xantphos)(**1**)]$^+$	365	570	1	12
[Cu(POP)(**2**)]$^+$	365	500	3	10
[Cu(xantphos)(**2**)]$^+$	365	500	3	10

[a] Solution concentration = 2.5×10^{-5} mol dm^{-3} for compounds with **1** and 2.5×10^{-6} mol dm^{-3} for compounds with **2**.

Table 5. Solid-state emission maxima, PLQY values and excited-state lifetimes for [Cu(PˆP)(NˆN)][PF$_6$] complexes in CH$_2$Cl$_2$ solutions.

Cation in [Cu(PˆP)(NˆN)][PF$_6$]	λ_{exc}/nm	λ_{em}/nm	PLQY/%	$\tau_{1/2}$/μs
[Cu(POP)(**1**)]$^+$	365	535	41	9.4
[Cu(xantphos)(**1**)]$^+$	365	560	35	11.1
[Cu(POP)(**2**)]$^+$	365	560	27	9.2
[Cu(xantphos)(**2**)]$^+$	365	577	19	5.0

4. Conclusions

We have described the synthesis and characterization of [Cu(PˆP)(**1**)][PF$_6$], [Cu(PˆP)(**2**)][PF$_6$] and [Cu(PˆP)(**3**)][PF$_6$] with the wide bite-angle PˆP ligands POP and xantphos. Solution multinuclear NMR spectroscopic data for the compounds are presented. The single crystal structures of [Cu(xantphos)(**1**)][PF$_6$]·CH$_2$Cl$_2$, [Cu(xantphos)(**2**)][PF$_6$]·CH$_2$Cl$_2$ and [Cu(POP)(**3**)][PF$_6$]·0.5H$_2$O were determined, confirming a distorted tetrahedral copper(I) coordination environment in each compound. The complex cations exhibit a range of intra- and inter-cation π-interactions. In both [Cu(xantphos)(**1**)][PF$_6$]·CH$_2$Cl$_2$, [Cu(xantphos)(**2**)][PF$_6$]·CH$_2$Cl$_2$, the NˆN and PˆP ligands engage in face-to-face π-stacking of bpy and PPh$_2$ phenyl rings. In [Cu(xantphos)(**2**)][PF$_6$]·CH$_2$Cl$_2$, inter-cation π-embraces lead to the formation of infinite chains as a primary packing motif. Packing of the [Cu(POP)(**3**)]$^+$ cations in [Cu(POP)(**3**)][PF$_6$]·0.5H$_2$O involves a combination of C–H . . . π (phenyl to bpy) and offset face-to-face (bpy . . . bpy) contacts. The compounds containing ligands **1** or **2** are green or yellow emitters in the solid-state (λ_{em} in the range 535–577 nm) with values of the PLQY in the range 19%–41%. For [Cu(xantphos)(**2**)][PF$_6$] and [Cu(POP)(**2**)][PF$_6$], a red-shift in the emission maximum on going from CH$_2$Cl$_2$ solutions to the solid-state is attributed to the extensive π-stacking between ligands **2** that is observed in the crystal structure of [Cu(xantphos)(**2**)][PF$_6$]·CH$_2$Cl$_2$.

References

1. Armaroli, N.; Accorsi, G.; Cardinali, F.; Listorti, A. Photochemistry and Photophysics of Coordination Compounds: Copper. *Top. Curr. Chem.* **2007**, *280*, 69–115. [CrossRef]
2. Costa, R.D.; Ortí, E.; Bolink, H.J.; Monti, F.; Accorsi, G.; Armaroli, N. Luminescent ionic transition metal complexes for light-emitting electrochemical cells. *Angew. Chem. Int. Ed.* **2012**, *51*, 8178–8211. [CrossRef] [PubMed]
3. Fresta, E.; Costa, R.D. Beyond traditional light-emitting electrochemical cells—A review of new device designs and emitters. *J. Mater. Chem. C* **2017**, *5*, 5643–5675. [CrossRef]
4. Costa, R.D. (Ed.) *Light-Emitting Electrochemical Cells: Concepts, Advances and Challenges*; Springer International Publishing: New York, NY, USA, 2017. [CrossRef]
5. Costa, R.D.; Tordera, D.; Ortí, E.; Bolink, H.J.; Schönle, J.; Graber, S.; Housecroft, C.E.; Constable, E.C.; Zampese, J.A. Copper(I) complexes for sustainable light-emitting electrochemical cells. *J. Mater. Chem. C* **2011**, *21*, 16108–16118. [CrossRef]

6. Buckner, M.T.; McMillin, D.R. Photoluminescence from copper(I) complexes with low-lying metal-to-ligand charge transfer excited states. *J. Chem. Soc. Chem. Commun.* **1978**, 759–761. [CrossRef]

7. Rader, R.A.; McMillin, D.R.; Buckner, M.T.; Matthews, T.G.; Casadonte, D.J.; Lengel, R.K.; Whittaker, S.B.; Darmon, L.M.; Lytle, F.E. Photostudies of 2,2′-bipyridine bis(triphenylphosphine)copper(1+), 1,10-phenanthroline bis(triphenylphosphine)copper(1+), and 2,9-dimethyl-1,10-phenanthroline bis(triphenylphosphine)copper(1+) in solution and in rigid, low-temperature glasses. Simultaneous multiple emissions from intraligand and charge-transfer states. *J. Am. Chem. Soc.* **1981**, *103*, 5906–5912. [CrossRef]

8. Keller, S.; Constable, E.C.; Housecroft, C.E.; Neuburger, M.; Prescimone, A.; Longo, G.; Pertegás, A.; Sessolo, M.; Bolink, H.J. [Cu(bpy)(PˆP)]$^+$ containing light-emitting electrochemical cells: Improving performance through simple substitution. *Dalton Trans.* **2014**, *43*, 16593–16596. [CrossRef]

9. Keller, S.; Pertegás, A.; Longo, G.; Martínez, L.; Cerdá, J.; Junquera-Hernández, J.M.; Prescimone, A.; Constable, E.C.; Housecroft, C.E.; Ortí, E.; et al. Shine bright or live long: Substituent effects in [Cu(NˆN)(PˆP)]$^+$-based light-emitting electrochemical cells where NˆN is a 6-substituted 2,2′-bipyridine. *J. Mater. Chem. C* **2016**, *4*, 3857–3871. [CrossRef]

10. Alkan-Zambada, M.; Keller, S.; Martínez-Sarti, L.; Prescimone, A.; Junquera-Hernández, J.M.; Constable, E.C.; Bolink, H.J.; Sessolo, M.; Ortí, E.; Housecroft, C.E. [Cu(PˆP)(NˆN)][PF$_6$] compounds with bis(phosphane) and 6-alkoxy, 6-alkylthio, 6-phenyloxy and 6-phenylthio-substituted 2,2′-bipyridine ligands for light-emitting electrochemical cells. *J. Mater. Chem. C* **2018**, *6*, 8460–8471. [CrossRef]

11. Brunner, F.; Graber, S.; Baumgartner, Y.; Häussinger, D.; Prescimone, A.; Constable, E.C.; Housecroft, C.E. The effects of introducing sterically demanding aryl substituents in [Cu(NˆN)(PˆP)]$^+$ complexes. *Dalton Trans.* **2017**, *46*, 6379–6391. [CrossRef]

12. Keller, S.; Prescimone, A.; Bolink, H.J.; Sessolo, M.; Longo, G.; Martínez-Sarti, L.; Junquera-Hernández, J.-M.; Constable, E.C.; Ortí, E.; Housecroft, C.E. Luminescent copper(I) complexes with bisphosphane and halogen-substituted 2,2′-bipyridine ligands. *Dalton Trans.* **2018**, *47*, 14263–14276. [CrossRef] [PubMed]

13. Keller, S.; Brunner, F.; Junquera-Hernández, J.M.; Pertegás, A.; La-Placa, M.-G.; Prescimone, A.; Constable, E.C.; Bolink, H.J.; Ortí, E.; Housecroft, C.E. CF$_3$ Substitution of [Cu(PˆP)(bpy)][PF$_6$] complexes: Effects on Photophysical Properties and Light-emitting Electrochemical Cell Performance. *ChemPlusChem* **2018**, *83*, 217–229. [CrossRef]

14. Leoni, E.; Mohanraj, J.; Holler, M.; Mohankumar, M.; Nierengarten, I.; Monti, F.; Sournia-Saquet, A.; Delavaux-Nicot, B.; Nierengarten, J.-F.; Armaroli, N. Heteroleptic Copper(I) Complexes Prepared from Phenanthroline and Bis-Phosphine Ligands: Rationalization of the Photophysical and Electrochemical Properties. *Inorg. Chem.* **2018**, *57*, 15537–15549. [CrossRef] [PubMed]

15. Brunner, F.; Martínez-Sarti, L.; Keller, S.; Pertegás, A.; Prescimone, A.; Constable, E.C.; Bolink, H.J.; Housecroft, C.E. Peripheral halo-functionalization in [Cu(NˆN)(PˆP)]+ emitters: Influence on the performances of light-emitting electrochemical cells. *Dalton Trans.* **2016**, *45*, 15180–15192. [CrossRef]

16. Norrby, T.; Börje, A.; Zhang, L.; Åkermark, B. Regioselective Functionalization of 2,2′-Bipyridine and Transformations into Unsymmetric Ligands for Coordination Chemistry. *Acta Chem. Scand.* **1998**, *52*, 77–85. [CrossRef]

17. Schönhofer, E.; Bozic-Weber, B.; Martin, C.J.; Constable, E.C.; Housecroft, C.E.; Zampese, J.A. 'Surfaces-as-ligands, surfaces-as-complexes' strategies for copper(I) dye-sensitized solar cells. *Dyes Pigment.* **2015**, *115*, 154–165. [CrossRef]

18. Constable, E.C.; Housecroft, C.E.; Kariuki, B.M.; Smith, C.B. Switching on Hydrogen Bonding in Oligopyridine Ligands. *Supramol. Chem.* **2006**, *18*, 305–309. [CrossRef]

19. Carroll, J.; Woolard, H.G.; Mroz, R.; Nason, C.A.; Huo, S. Regiospecific acylation of cycloplatinated complexes. Scope, limitation, and mechanistic implications. *Organometallics* **2016**, *35*, 1313–1322. [CrossRef]

20. Kubas, G.J. Tetrakis(acetonitrile)copper(I) hexafluorophosphate. *Inorg. Synth.* **1979**, *19*, 90–92. [CrossRef]

21. *Software for the Integration of CCD Detector System*; Bruker Analytical X-ray Systems, Bruker axs: Madison, WI, USA, 2013.

22. Sheldrick, G.M. ShelXT-Integrated space-group and crystal-structure determination. *Acta Crystallogr.* **2015**, *71*, 3–8. [CrossRef]

23. Dolomanov, O.V.; Bourhis, L.J.; Gildea, R.J.; Howard, J.A.K.; Puschmann, H. Olex2: A Complete Structure Solution, Refinement and Analysis Program. *J. Appl. Cryst.* **2009**, *42*, 339–341. [CrossRef]

24. Sheldrick, G.M. Crystal Structure Refinement with ShelXL. *Acta Cryst.* **2015**, *71*, 3–8.

25. Macrae, C.F.; Edgington, P.R.; McCabe, P.; Pidcock, E.; Shields, G.P.; Taylor, R.; Towler, M.; van de Streek, J. Mercury: Visualization and Analysis of Crystal Structures. *J. Appl. Cryst.* **2006**, *39*, 453–457. [CrossRef]

26. Macrae, C.F.; Bruno, I.J.; Chisholm, J.A.; Edgington, P.R.; McCabe, P.; Pidcock, E.; Rodriguez-Monge, L.; Taylor, R.; van de Streek, J.; Wood, P.A. Mercury CSD 2.0—New Features for the Visualization and Investigation of Crystal Structures. *J. Appl. Cryst.* **2008**, *41*, 466–470. [CrossRef]

27. Yang, L.; Powell, D.R.; Houser, R.P. Structural variation in copper(I) complexes with pyridylmethylamide ligands: Structural analysis with a new four-coordinate geometry index, τ_4. *Dalton Trans.* **2007**, 955–964. [CrossRef]

28. Janiak, C. A critical account on π–π stacking in metal complexes with aromatic nitrogen-containing ligands. *J. Chem. Soc. Dalton Trans.* **2000**, 3885–3896. [CrossRef]

29. Groom, C.R.; Bruno, I.J.; Lightfoot, M.P.; Ward, S.C. The Cambridge Structural Database. *Acta Cryst.* **2016**, *B72*, 171–179. [CrossRef]

30. Brunner, F.; Babaei, A.; Pertegás, A.; Junquera-Hernández, J.M.; Prescimone, A.; Constable, E.C.; Bolink, H.J.; Sessolo, M.; Ortí, E.; Housecroft, C.E. Phosphane tuning in heteroleptic [Cu(NˆN)(PˆP)]$^+$ complexes for light-emitting electrochemical cells. *Dalton Trans.* **2019**, *48*, 446–460. [CrossRef]

31. Weber, M.D.; Viciano-Chumillas, M.; Armentano, D.; Cano, J.; Costa, R.D. σ-Hammett parameter: A strategy to enhance both photo- and electro-luminescence features of heteroleptic copper(II) complexes. *Dalton Trans.* **2017**, *46*, 6312–6323. [CrossRef]

32. Dance, I.; Scudder, M. Supramolecular motifs: Sextuple aryl embraces in crystalline [M(2,2′-bipy)$_3$] and related complexes. *J. Chem. Soc. Dalton Trans.* **1998**, 1341–1350. [CrossRef]